Color from hierarchy: Diverse optical properties of micron-sized spherical colloidal assemblies

Nicolas Vogel[a,b,c,1], Stefanie Utech[a], Grant T. England[a], Tanya Shirman[a,d], Katherine R. Phillips[e], Natalie Koay[d], Ian B. Burgess[d,f], Mathias Kolle[g], David A. Weitz[a], and Joanna Aizenberg[a,d,e]

[a]John A. Paulson School of Engineering and Applied Sciences, Harvard University, Cambridge, MA 02138; [b]Institute of Particle Technology, Friedrich-Alexander-University Erlangen–Nürnberg, 91058 Erlangen, Germany; [c]Cluster of Excellence Engineering of Advanced Materials, Friedrich-Alexander-University Erlangen–Nürnberg, 91054 Erlangen, Germany; [d]Wyss Institute for Biologically Inspired Engineering, Harvard University, Cambridge, MA 02138; [e]Department of Chemistry and Chemical Biology, Harvard University, Cambridge, MA 02138; [f]Leslie Dan Faculty of Pharmacy, University of Toronto, Toronto, Canada, M5S 3M2; and [g]Department of Mechanical Engineering, Massachusetts Institute of Technology, Cambridge, MA 02139

Edited by Radislav A. Potyrailo, General Electric Co., Niskayuna, NY, and accepted by the Editorial Board July 28, 2015 (received for review March 30, 2015)

Materials in nature are characterized by structural order over multiple length scales have evolved for maximum performance and multifunctionality, and are often produced by self-assembly processes. A striking example of this design principle is structural coloration, where interference, diffraction, and absorption effects result in vivid colors. Mimicking this emergence of complex effects from simple building blocks is a key challenge for man-made materials. Here, we show that a simple confined self-assembly process leads to a complex hierarchical geometry that displays a variety of optical effects. Colloidal crystallization in an emulsion droplet creates micron-sized superstructures, termed photonic balls. The curvature imposed by the emulsion droplet leads to frustrated crystallization. We observe spherical colloidal crystals with ordered, crystalline layers and a disordered core. This geometry produces multiple optical effects. The ordered layers give rise to structural color from Bragg diffraction with limited angular dependence and unusual transmission due to the curved nature of the individual crystals. The disordered core contributes nonresonant scattering that induces a macroscopically whitish appearance, which we mitigate by incorporating absorbing gold nanoparticles that suppress scattering and macroscopically purify the color. With increasing size of the constituent colloidal particles, grating diffraction effects dominate, which result from order along the crystal's curved surface and induce a vivid polychromatic appearance. The control of multiple optical effects induced by the hierarchical morphology in photonic balls paves the way to use them as building blocks for complex optical assemblies—potentially as more efficient mimics of structural color as it occurs in nature.

self-assembly | colloids | photonic crystal | structural color | hierarchy

Hierarchical design principles, i.e., the structuration of material over multiple length scales, are ubiquitously used in nature to maximize functionality from a limited choice of available components. Hierarchically structured materials often provide better performance than their unstructured counterparts and novel properties can arise solely from the multiscale structural arrangement. Examples can be found in the extreme water repellency of the lotus leaf (1); the outstanding mechanical stability and toughness of sea creatures such as sea sponges (2) and abalone shells (3); and the bright coloration found in beetles, birds, and butterflies (4, 5).

To achieve the strongest visual effects, many organisms combine optical effects arising from light interacting with structured matter at different length scales (6). Structural periodicity on the scale of visible light wavelengths can result in regular optical density variations that give rise to bright, iridescent colors due to pronounced interference effects (4). At the micron scale, regular structural features act as diffraction gratings that produce vivid, rainbow coloration (7) and are used to control scattering (8) and to direct the emission of light by mirror-like reflections (9). At the molecular level, broadband absorption, for example by melanin, can be used to reduce unwanted scattering due to structural imperfections, which, if not eliminated, can lead to a whitish appearance (10).

Several advantages of structural coloration compared with pigmentation hues have led to a strong interest in mimicking nature's photonic design principles in technology (11, 12). These advantages include increased color longevity by the absence of photobleaching; the ability to use benign and nontoxic materials; broad variation in colors arising from simple changes in geometry of the same material; and the presence of vivid optical effects such as sparkle, luster, and iridescence, not achievable by conventional pigments. However, structural color requires a high degree of control over the nano- and microscale geometry of the colored material. Self-assembly processes involving colloidal particles have been identified as an attractive route to create ordered structures at the nanoscale without the need for expensive and serial nanofabrication methods (13–15). Colloidal particles are attractive building blocks for mimicking nature's structural coloration strategies because they can be conveniently synthesized in a range of sizes comparable to those of visible light wavelengths. Colloids self-assemble into highly ordered, close-packed crystals on flat surfaces, giving rise to structural color by constructive interference of light reflected at the individual lattice planes (13, 15).

Structural hierarchy, i.e., the organization of colloidal crystals into ordered superstructures, can be achieved by imposing a confining element on the crystallization process. A simple yet

Significance

Controlling the internal structure over multiple length scales can produce materials with superior properties. This hierarchical design is ubiquitous in nature where materials have evolved to show maximum functionality from a limited choice of available building blocks. Mimicking the emergence of functionality from simple building blocks is a key challenge for man-made materials. Here, we show how a simple confined self-assembly of colloidal particles leads to a complex geometry that displays a surprising variety of optical effects. These effects are a result of the intricate interaction of light with the structural features at different length scales, and the geometry of the self-assembled structure. The results underline the importance of controlling assembly processes over multiple length scales to tailor properties and maximize performance.

Author contributions: N.V. and J.A. designed research; N.V., S.U., G.T.E., K.R.P., N.K., I.B.B., and M.K. performed research; G.T.E. and T.S. contributed new reagents/analytic tools; N.V., S.U., G.T.E., I.B.B., M.K., D.A.W., and J.A. analyzed data; and N.V. and J.A. wrote the paper.

The authors declare no conflict of interest.

This article is a PNAS Direct Submission. R.A.P. is a guest editor invited by the Editorial Board.

[1]To whom correspondence should be addressed. Email: nicolas.vogel@fau.de.

This article contains supporting information online at www.pnas.org/lookup/suppl/doi:10.1073/pnas.1506272112/-/DCSupplemental.

interesting confinement for the crystallization process is an emulsion droplet that creates colloidal assemblies known as photonic balls (16–19). Curvature imposed by the spherical confinement is a unique structural element of photonic balls. It is known that curvature induces different types of defect structures in 2D (20, 21) and 3D assemblies (22), which can affect the resulting optical properties. Photonic balls have recently gained attention in various optical applications, including pigments (23–26), sensors (27), magnetically switchable colorants (25, 28), and color-coded substrates for biomaterials evaluation (29, 30).

Here, we provide a detailed physical understanding of the different optical phenomena occurring in photonic balls and trace the origin of these properties to structural details, especially curvature. We use focused ion beam-assisted cross-sectioning to visualize the effect of confinement on the internal morphology and find ordered, layered crystal planes near the interface and a more disordered region toward the center. Tailoring the degree of confinement allows us to control the crystallinity and thus, the resulting color arising from Bragg diffraction. Disorder and defects, caused by frustrated crystallization in the curved confinement, contributes to unwanted broadband scattering of light, which compromises the macroscopic color. We introduce gold nanoparticles as subwavelength, spectrally selective absorbers into the photonic balls to suppress light scattering in spectrally unwanted regions. This synergistic combination of plasmonic absorption with Bragg diffraction leads to a macroscopically purer coloration, if the photonic crystal stop band and gold nanoparticle absorption are appropriately adjusted. Finally, we observe more complex optical signatures in the reflection of light from photonic balls assembled from larger colloidal particles ($d > 400$ nm) that result from grating diffraction caused by a regular arrangement of colloids at the surface of the photonic balls.

Our theoretical experimental examination of the influence of curvature and confinement on the different optical phenomena enables us to create a complete picture of the rich optical properties of these simple, hierarchical self-assembled structures.

Results and Discussion

Synthesis and Internal Morphology of Photonic Balls. We use droplet-based microfluidics to emulsify an aqueous dispersion of polystyrene colloids in a continuous fluorocarbon oil phase (31). The cross-junction devices are conveniently prepared from poly(dimethylsiloxane) (PDMS) by soft lithography and enable us to create stable emulsions with narrow size distributions in a continuous-flow process as illustrated in Fig. 1*A* (32). After emulsification, the water is removed from the generated droplets at 45 °C, resulting in shrinkage of the emulsion droplets and self-assembly of the colloids in their spherical confinement. We control the diameter of the produced photonic balls from below 10 μm to above 100 μm by tuning the concentration of colloids in the aqueous dispersion and the size of the emulsion droplet generated in the microfluidic device (Fig. S1). The surface of the balls, visible in Fig. 1 *B* and *C*, shows colloids ordered in a polycrystalline, close-packed lattice, previously assigned as the (111) lattice plane of the 3D crystal formed in the spherical confinement (23, 24). However, the curvature in the confinement impedes the formation of a perfectly ordered crystal, resulting in characteristic defects and assembly structures (20, 21). A focused ion beam (FIB) was used to cross-section photonic balls and uncover their internal crystal structure, which we show in Fig. 1*D* and Fig. S2. The cross-sections reproducibly indicate the presence of a layered morphology of the colloidal crystal toward the interface, consisting of several close-packed [i.e., (111)] planes stacked into a curved 3D crystal. Towards the center of the ball, the assembly appears increasingly disordered, presumably as a consequence of increasing frustration. The higher the level of confinement is (i.e., the smaller the ratio of the diameters of ball and colloid, d_{ball}/d_{coll}), the fewer ordered layers exist (Fig. S2). It is worth noting that the structures we observe seem less faceted and appear to follow the curvature of the confinement more than would be expected from thermodynamic considerations (22), indicating that kinetic effects may play a significant role in our system.

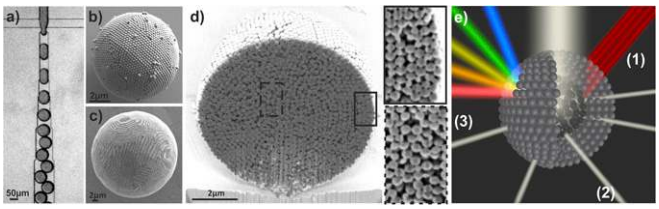

Fig. 1. Photonic balls are prepared by self-assembly of colloids in the spherical confinement of emulsion droplets. (*A*) Optical micrograph of the cross-junction microfluidic device used to emulsify a colloidal dispersion into monodisperse droplets. (*B* and *C*) SEM micrographs of photonic balls formed by assembly of 250-nm colloids in the confinement of an emulsion droplet (d_{ball} = 8 μm in *B* and 30 μm in *C*). Moiré patterns visible in *C* indicate high order. (*D*) Exemplary cross section of a photonic ball obtained by FIB cutting indicates a layered internal morphology with ordered structure around the interface (*Top Inset*) and increasing disorder toward the center (*Bottom Inset*). See Fig. S2 for further examples. (*E*) Schematic illustration of multiple optical effects originating from the hierarchical self-assembly (*1*): Crystalline order results in Bragg reflection of light with a wavelength defined by the colloid size (*2*); disorder in the assembly gives rise to unselective scattering of incident light (*3*); periodic assemblies at the ball's surface lead to grating diffraction effects, separating white light into its spectral components (for colloid sizes >400 nm).

This curved crystal structure relates to multiple optical properties observed in photonic balls, as schematically illustrated and labeled in Fig. 1*E*. We estimate the amount of order present in photonic balls of a given size based on the intensity of structural coloration that we observe from Bragg diffraction at the ordered lattice planes "(*1*)". We show that broadband scattering of light, caused by the photonic ball dimensions and the internal disorder, induces a whitish macroscopic appearance "(*2*)", which can be mitigated by incorporating gold nanoparticles. Finally, we identify the ordered arrangement of colloids at the surface of the photonic ball as the origin of color from grating diffraction "(*3*)".

Coloration Arising from Bragg Diffraction. We investigate the color of individual photonic balls, using a fiber-optic cable to collect and spectrally analyze reflected light of individual photonic balls through a microscope objective lens. Fig. 2*A* shows optical images and corresponding measured reflection spectra (solid lines) of individual balls (d_{ball} = 30 μm) consisting of colloids with sizes of 180 nm, 225 nm, and 250 nm that display blue, green, and red structural color, respectively. This color has been previously assigned to Bragg diffraction, i.e., constructive interference of light reflected at individual lattice planes in the curved colloidal crystal (23). The FIB cross sections (Fig. 1*D* and Fig. S2) confirm the presence of such layers in our system. A consequence of the spherical nature of the photonic balls is the lack of angular dependence under illumination conditions in a microscope as shown in Fig. 2*B*.

We model the photonic balls as a multilayer structure in a 1D transfer matrix simulation with a refractive index profile corresponding to a stacked, close-packed colloidal crystal (details in Fig. S3). The simulated spectra, shown as dotted lines in Fig. 2*A*, match the experiments, corroborating that multilayer interference at stacked (111) planes can cause the observed color. To match the peak intensity, simulations were performed assuming seven (180-nm colloids) and nine (225-nm and 250-nm colloids) perfectly ordered layers of colloidal crystal.

The most prominent feature of the optical microscope images throughout Fig. 2 is an area with intense, uniform color in the center of the ball surrounded by a pale, almost colorless rim. We attribute this color pattern to the spherical nature of the hierarchical assembly: Only the center of the photonic ball

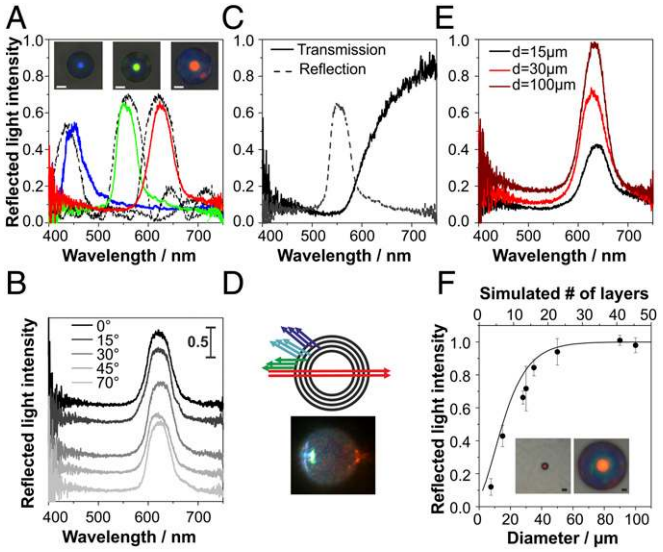

Fig. 2. Optical properties arising from Bragg diffraction of light at ordered crystal layers. (*A*) Structural color can be tuned throughout the visible spectrum (solid lines: blue, d_{coll} = 180 nm; green, d_{coll} = 225 nm; red, d_{coll} = 250 nm; photonic ball diameter is 30 μm in all cases) and correlates with 1D simulations (dotted lines) of light reflection at stacked (111) planes within the ball. (*B*) Reflected light intensity and wavelengths are spectrally independent of the angle of incidence with respect to the substrate surface. (*C* and *D*) The transmission spectra of a photonic ball (250-nm colloids) resembles a long-pass filter, which can be explained by the curved nature of the ball and directly visualized by illumination from the side (*D*). (*E* and *F*) The reflected light intensity depends on the size of the photonic balls and reaches saturation for balls with a diameter of 50 μm and larger. The intensity correlates with an increase in the number of ordered layers obtained from simulations (solid line) (*F*). (All scale bars, 10 μm.) *F, Insets* show photonic balls with a diameter of 8 μm (*Left*) and 100 μm (*Right*).

reflects light that can be detected in the microscope objective (Fig. S4*A*). Larger angles of incident and reflected light—causing a blue shift of color—are not picked up by the microscope objective (Fig. S4*A*), creating the observed uniform coloration. The colorful area of the ball corresponds to the angular range of back-reflected light the objective can collect, which we confirmed by imaging an individual photonic ball with objectives of different numerical aperture and found quantitative agreement between the accessible angles calculated from the numerical aperture of the lens and from the ratio of the colored area to the ball diameter (Figs. S4*B* and S5 and Table S1). However, this model does not account for colored patches visible at the outer rims of some photonic balls, e.g., in the red-colored ball in Fig. 2*A*. These spots may be caused by light reflected back into the objective at ordered planes perpendicular to the stacked (111) planes, visible in cross-sectional images (Fig. S4*C*).

Unlike typical thin film photonic crystals, photonic balls exhibit transmission spectra that are not the inverse of the reflection; instead, only light above a critical threshold wavelength is transmitted, whereas light with energies higher than the observed reflection peak seems unable to pass the structure (Fig. 2*C*). Again, we attribute this unexpected behavior to the curved nature of the crystal, as schematically illustrated in Fig. 2*D*. Even though only light reflected normal to the ball's surface is picked up in the reflection spectrum (resulting in a green reflection peak in the illustration), reflections also occur at different angles (although they are not picked up by the microscope as described above). Such reflections will have a larger angle between incident and reflected light, which translates to constructive interference occurring at lower wavelengths (i.e., cyan and blue light in the illustration) (33). Therefore, only light with wavelengths higher than the threshold defined by the constructive interference at normal incidence is transmitted, leading to the transmission characteristics shown in Fig. 2*C*. This phenomenon can be observed directly, if a photonic ball is illuminated from the (Fig. 2*D*).

The size of the photonic balls, and thus the confinement of the colloids, can easily be controlled synthetically. Fig. 2*E* exemplarily shows reflection spectra of photonic balls prepared from 250-nm colloids with a size of 15 μm, 30 μm, and 100 μm (to-scale microscope images are shown in Fig. 2*F*, *Insets*). With increasing size of the photonic ball, the intensity of the Bragg reflection peak increases and reaches values close to saturation for balls with a size of 50 μm (Fig. 2*F*). This indicates an increase in crystallinity as a result of a less severe confinement with increasing ball size. We then compare the measured reflected light intensity for different ball diameters with simulated values of multilayer reflection with increasing numbers of crystalline layers (Fig. 2*F*). The measured reflectivities closely follow the simulated values, indicating that the amount of order is directly correlated to the degree of confinement. Consequently, we can use optical information to indirectly assess the degree of internal order of individual photonic balls by comparing the measured and simulated intensity of reflected light.

Mitigating Scattering by Incorporation of Spectrally Selective Absorbers. The spherical confinement of the photonic balls inherently induces disorder in the colloidal arrangement, leading to a whitish appearance due to scattering. To create structural color with high chromatic values, the nonresonant scattering needs to be controlled. The addition of broadband absorbers (for example, carbon black) can suppress scattering, increasing the contrast between spectral background and Bragg diffraction peak (34, 35). However, the Bragg peak itself can decreased as well due to the unselective nature of absorption. In contrast, light absorption of noble metal nanoparticles at their plasmon resonance frequency occurs over a rather narrow part of the visible spectrum and can be tuned by changing size and shape of the metal nanoparticle (36). Such nanoparticles can serve as spectrally selective absorbers that absorb scattered light at undesired wavelengths (37). Most importantly, their absorption frequency can be tailored to minimize interference with the Bragg diffraction peak of the photonic crystal. This leads to a purification of the optical spectrum by suppression of the intensity of scattered light from undesired parts of the spectrum with minor effects on the intensity of the Bragg peak.

Here, we use 12-nm gold nanoparticles (details in *SI Materials and Methods*) to mitigate the whitish appearance caused by the presence of disorder, producing a more crisp red coloration as demonstrated in Fig. 3. Due to their small size, the gold nanoparticles do not interfere with the assembly of the colloidal particles, enabling the creation of hybrid photonic–plasmonic balls (38). Fig. 3 *A*–*C* shows single-particle spectra of three different types of such hybrid balls. A disordered ball containing gold nanoparticles, prepared by mixing two populations of colloidal particles with diameters of 200 nm and 250 nm chosen to induce disorder by lattice mismatch, does not show a Bragg reflection peak (Fig. 3*A*). The plasmon resonance of the gold nanoparticles leads to a dip in the reflection spectrum at 520 nm, indicated by an arrow in Fig. 3*A*, resulting in a dull, reddish appearance. An ordered photonic ball, consisting of 250-nm colloids without gold nanoparticles, is shown in Fig. 3*B*, with a red color stemming from the Bragg diffraction peak at 600 nm. Figure 3*B* shows a photonic ball without gold nanoparticles that shows a Bragg diffraction peak at 620 nm. The addition of gold nanoparticles to an ordered photonic ball (Fig. 3*C*) combines the two spectral features: A dip in reflection, caused by the plasmon resonance, lowers the reflected light intensity in the lower-wavelength (blue/green) part of the spectrum but does not affect the higher-wavelength (red) region with the Bragg peak. Theoretical investigations reveal that the position of the gold

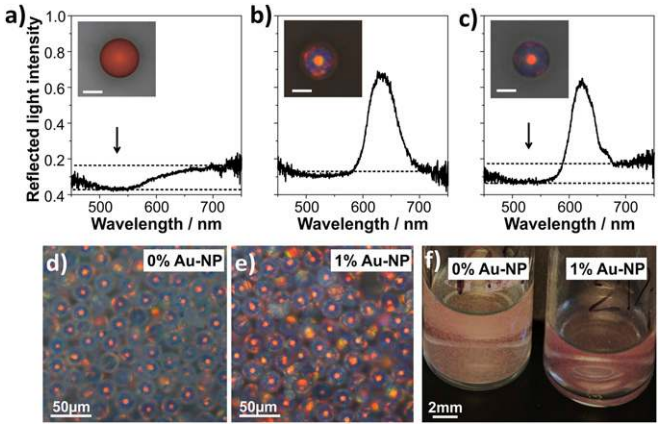

Fig. 3. Color purification by incorporation of spectrally selective absorbers. (*A*) Reflection spectra of a disordered photonic ball (binary mixture of colloids with d = 200 nm and 250 nm) with 12-nm Au nanoparticles (NPs). The absorption of the Au NPs lowers the reflection of light in the blue/green part of the spectrum (arrow), giving the ball a dull, red appearance (*A*, *Inset*). (*B*) An ordered photonic ball ($d_{colloids}$ = 250 nm) shows a Bragg reflection peak at 620 nm, leading to a bright, red color (*Inset*). (*C*) An ordered photonic ball with gold nanoparticles shows lowered reflection at the blue/green part of the spectrum without affecting the Bragg reflection peak. (*D*–*F*) Control of scattering properties by addition of Au NPs in ensembles of photonic balls. Microscopic images (*D* and *E*, taken with identical exposure times) and macroscopic images (*F*) reveal an increased contrast.

nanoparticles within the ball strongly influences the purification effect: Positioning the particles within the ordered parts of the photonic structures increases color saturation whereas absorbers placed selectively in the disordered part decrease color saturation (Fig. S6). Simulations reveal an optimal absorber concentration of approximately 15% gold by volume (Fig. S6), when gold nanoparticles are placed exclusively in an idealized, ordered colloidal crystal.

The effect of nanoparticle addition becomes much more apparent in ensembles of photonic balls. Microscope images taken with identical exposure times, shown in Fig. 3 *D* and *E*, as well as a macroscopic photograph (Fig. 3*F*) reveal a whitish appearance of plain photonic balls due to unselective light scattering. The selective suppression of scattered light at lower wavelengths by absorption of light by the gold nanoparticles increases the contrast with little effect on the color intensity, resulting in a macroscopically more crisp color.

Coloration Arising from Grating Diffraction. Photonic balls assembled from colloids with a diameter above 400 nm show color patterns that differ substantially from their analogs with smaller colloid sizes. Bright, multichromatic color patches appear at the outer regions of the photonic ball, showing color travel from blue to red with increasing distance from the center. This contrasts with the uniform coloration with colorless rims observed for photonic balls from colloids with sizes smaller than 400 nm. Previously, such color patterns in larger colloid assemblies were attributed to Bragg diffraction from different crystal planes (24) and grating diffraction effects (38). Here, we present further evidence that Bragg diffraction from different crystal planes is an unlikely origin of color patterns and that diffraction-grating effects, arising from periodic arrangements of colloids at the surface of our micron-scale photonic balls, are responsible for the optical effect. A representative SEM image (ball diameter 15 µm), highlighting the ordered, close-packed arrangement of 400-nm colloids at the surface of the spherical superstructure, is shown in Fig. 4*A*. A microscope image of a larger photonic ball (d = 100 µm) from similar-sized colloids, shown in Fig. 4*B*, shows strong rainbow colors extending toward the rim. The lateral distribution of colors is not affected by the ball size (38) and can be seen in all samples with photonic ball diameters between 15 µm and 100 µm (Fig. S7). Clearly, the coloration is characterized by a gradual change from blue to red. Such a color travel is characteristic of grating diffraction, as described by the grating equation, $m\lambda = d(\sin\theta_i + \sin\theta_m)$ (39). For each diffraction order m, the wavelength of constructive interference (λ) changes with increasing angles of incident light (θ_i) and reflected light (θ_m) and with the distance (d) between the individual scatterers. In contrast, were the colors to arise from Bragg diffraction at different crystal planes, few distinctive colors would be observed.

To resolve the origin of the coloration, we model the surface of a photonic ball as a regularly spaced arrangement of spheres on a hemispherical substrate, as shown in Fig. 4*C*. We assume that the colloids serve as a curved diffraction grating and calculate the angular distributions of constructively interfering waves for different colors from the grating equation for different positions along the surface. Although the illumination is fixed from the top (normal to the substrate plane), the angle that the incoming light beam forms with the ball's surface differs at different positions as a result of the curved nature of the photonic ball. It is necessary to keep in mind that only light reflected in a small range of angles given by the numerical aperture around the surface normal (with respect to the substrate plane, not the ball surface) is collected by the microscope objective lens (indicated by dotted cones in Fig. 4*C*). Colors that are visible in the microscope image must therefore be reflected at angles within this cone. Because the angle of incident light with the curved surface changes with increasing distance from the center, so does the wavelength of light constructively interfering at angles that can be picked up by the objective lens. As we move the beam away from the center (Fig. 4 *C*, *1*), grating diffraction predicts the shortest wavelength (blue light, modeled at 400 nm) to be picked up by the microscope first (Fig. 4 *C*, *2*). With increasing distance from the center, the light arriving in the microscope changes gradually along the visible spectrum via green (550 nm, Fig. 4 *C*, *3*) toward red (750 nm), which the model predicts to reach the objective lens only by reflection close to the rim (Fig. 4 *C*, *4*).

To facilitate comparison between model and experimentally observed coloration, we present the results of the model in a top-view representation in Fig. 4*D*. Light of a given wavelength that is collected by the microscope objective at a given distance from the center is represented by a colored dot. We choose to illustrate the

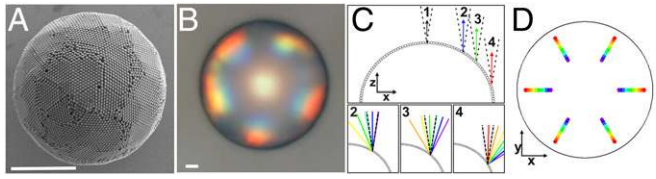

Fig. 4. Observation of grating diffraction from the periodic surface structures of photonic balls. (*A* and *B*) SEM and optical micrographs of photonic balls prepared from 400-nm colloids. Diffraction-grating colors, arising from the periodic arrangements of the colloids at the ball's surface, are visible toward the rims of the ball. (Scale bars, 10 µm.) (*C*) Model of the photonic ball's surface as a one-dimensional, curved diffraction grating and angular distribution of colors at different parts of the curved surface. Only light that is reflected back with a small range of angles (defined by the N.A. of the objective, indicated as a dotted cone in the image) close to normal to the surface from the grating is picked up by the objective lens and appears as color on the ball's surface. Because the incident angle increases from point *1* to point *4*, light with increasing wavelengths is back-reflected into the lens. (*D*) Spatial distribution of the color predicted by the model, plotted on a circular surface mimicking the top-view image of the ball. The positions of color in the model and micrograph coincide.

data obtained by the 1D model on the surface of a disk, representing the photonic ball as seen in a microscope, and assign a sixfold symmetry for the color map to depict the symmetry of a colloidal crystal. Image analysis, performed by measuring the distance of different color patches from the center of the photonic ball, reveals quantitative agreement on the color position between model and experiment (Table S2).

From the grating diffraction model, we expect a shift of the diffracted colors toward lower angles with larger periodicities. For the photonic balls, this translates into a shift of the rainbow-colored patches toward the center of the ball if the size of the constituent colloids is increased (38). The theory also predicts the appearance of higher-diffraction orders at larger angles (39), which should be observed at locations farther from the center of the ball. Indeed, both features are visible in the optical micrographs shown in Fig. 5. Photonic balls assembled from 610-nm colloids illuminated from the top and side are shown in Fig. 5 *B* and *C*, with a second grating order visible toward the rim of the structure. The position of the individual colors again coincides with the model quantitatively (Table 1 and Fig. S8). More remarkably, in photonic balls from 1,060-nm colloids (Fig. 5 *F* and *G*), three diffraction orders are visible and can be correlated with the model (Fig. 5, Table S2, and Fig. S8). The color patches assigned to the individual diffraction orders in the model (Fig. 5 *D* and *H*) are offset for better visibility.

To unambiguously assign the observed color to grating diffraction and not Bragg diffraction (24, 38), we coat large, 50-μm polystyrene microbeads with a monolayer of 610-nm colloids—the same particles used to assemble the photonic balls in Fig. 4 *A*–*C*—following a protocol from the literature (40). This monolayer-on-microbead architecture, shown in Fig. 5*I*, mimics the surface of a photonic ball but not its crystalline interior. Therefore, it cannot show Bragg diffraction. However, in the optical microscope image shown in Fig. 5*J*, we observe similar color patterns to those for the 3D photonic ball, with matching lateral position of the colors (Table 1). Therefore, we conclude that we indeed observe diffraction-grating effects on individual microscale photonic balls.

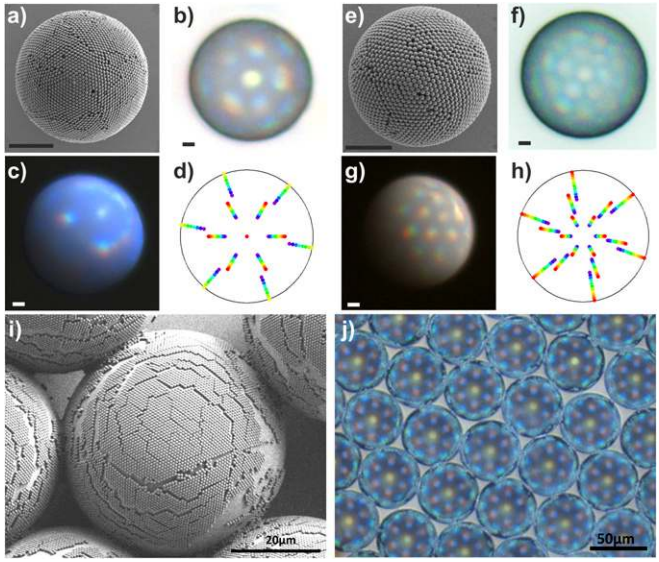

Fig. 5. Multiple diffraction orders are observed in photonic balls from larger colloids. (*A*–*D*) SEM micrograph (*A*) and optical properties (*B* and *C*) of photonic balls prepared from 610-nm colloids. Two diffraction orders are visible as polychromatic spots in the optical micrographs in top (*B*) and side (*C*) illumination. The positions of the colors on the ball coincide with theoretical expectations based on a 1D model of grating diffraction on a curved surface (*D*). (*E*–*H*) SEM micrograph (*E*) and optical properties (*F* and *G*) of photonic balls prepared from 1,060-nm colloids. The optical micrographs in top (*F*) and side (*G*) illumination show three diffraction orders, the position of which coincides with theoretical expectations (*H*). The color patches assigned to the individual diffraction orders in the model are slightly offset for better visibility. (All scale bars, 10 μm.) (*I* and *J*) SEM and optical micrographs of a close-packed monolayer of 610-nm colloids deposited onto a 50-μm bead, mimicking the periodic arrangement of the colloids at the surface of a photonic ball. The monolayer-on-microbead architecture shows similar coloration, implying that grating diffraction is the origin of the color.

Table 1. Lateral positions of selected colors observed experimentally (r_{meas}) and calculated from the diffraction-grating equation (r_{calc}) for 3D photonic balls and monolayer-on-microsphere architecture (both from 610-nm colloids)

D.O.	λ, nm	r_{calc}/r_{ball}	r_{meas}/r_{ball}	Discrepancy, %
Photonic balls (d_{coll} = 610 nm)				
1	400	0.33	0.30 ± 0.03	9.7
	550	0.45	0.46 ± 0.04	3.0
	750	0.61	0.69 ± 0.05	13.7
2	400	0.66	0.62 ± 0.04	5.0
	550	0.90	0.81 ± 0.05	10.5
Monolayer-on-microbead architecture (d_{coll} = 610 nm)				
1	400	0.33	0.27 ± 0.01	16.3
	550	0.45	0.45 ± 0.04	0.7
	750	0.61	0.73 ± 0.03	19.3
2	400	0.66	0.65 ± 0.02	1.4
	550	0.90	0.81 ± 0.05	10.8

Data are presented as fractions of the ball radius r_{ball} for the different diffraction orders (D.O.).

Conclusion

We explore how hierarchical order influences the properties of a self-assembled structure by studying individual microscale spherical colloidal crystals, known as photonic balls. Curvature, imposed on the colloidal crystal through the spherical confinement of an emulsion droplet, is the key element that alters the properties of the assembly. We provide a complete physical understanding of all optical effects observable in the prepared photonic balls and connect them to their structural origins.

FIB-assisted cross-sectioning indicates a layered morphology in the photonic balls that consists of radially ordered layers stacked from the interface toward the interior and a more disordered assembly towards the center. The layered structure gives rise to structural coloration by Bragg diffraction. When observed in a microscope, the presence of curvature creates uniform, angle-independent colors with a distinct colored ball area that reflects the numerical aperture of the objective. In contrast to flat opal films, the transmission spectra of a photonic ball are not the inversion of the reflection spectra but resemble a long-pass filter—again caused by reflection of light from the curved crystal. We control the degree of crystallinity via the size of the photonic balls and correlate the internal structure with the observed color intensity. Furthermore, we show that gold nanoparticles can be used as spectrally selective absorbers to suppress scattering, leading to a macroscopically brighter color. We present evidence that photonic balls assembled from colloids with a diameter of 400 nm or larger show diffraction-grating coloration arising from the periodic arrangement of colloids at the surface of the particles.

We anticipate these results will lead to several research directions. First, additional insight into crystallization in spherical confinements, especially with respect to the crystallization mechanism and its kinetics, is needed to understand and control the assembly of colloids into spherical superstructures. Second, if the quality of the photonic balls can be reproducibly provided, they may serve as interesting materials for potential use as miniaturized photonic elements, for example as long-pass filters, diffraction gratings, or colorimetric sensors; in (optical) laboratory-on-a-chip applications; or as dispersible structural color pigments. Finally,

the use of photonic balls as building blocks to create higher levels of hierarchy by self-assembly into more complex superstructures is a promising approach to further refine and exploit their rich optical properties.

Materials and Methods

Colloidal particles were synthesized by surfactant-free emulsion polymerization with acrylic acid as comonomer (41). PEG-modified gold nanoparticles with a size of 12 nm were synthesized by reduction of sodium tetrachloroaurate (Fig. S9) as described in the literature (42). Microfluidic devices were prepared by soft lithography from masters prepared by photolithography (31). Simulation of the optical properties was performed as a 1D transfer matrix method implemented in Matlab and effects of gold nanoparticles were included by adjusting the refractive index profile (43). Optical spectra of individual photonic balls were measured through a microscope objective lens. All procedures are described in detail in *SI Materials and Methods*.

ACKNOWLEDGMENTS. This work was supported by the National Science Foundation Materials Research Science and Engineering Center at Harvard University under Award DMR-1420570 and by the Badische Anilin und Sodafabrik's North American Center for Research on Advanced Materials. N.V. acknowledges funding of the Deutsche Forschungsgemeinschaft (DFG) through the Cluster of Excellence Engineering of Advanced Materials. S.U. acknowledges funding from DFG. K.R.P. acknowledges support from a graduate research fellowship from the Department of Defense. I.B.B. acknowledges support from a Banting Postdoctoral Fellowship funded by the Natural Sciences and Engineering Research Council of Canada. M.K. acknowledges financial support from the Massachusetts Institute of Technology Mechanical Engineering Department.

1. Barthlott W, Neinhuis C (1997) Purity of the sacred lotus, or escape from contamination in biological surfaces. *Planta* 202(1):1–8.
2. Aizenberg J, et al. (2005) Skeleton of Euplectella sp.: structural hierarchy from the nanoscale to the macroscale. *Science* 309(5732):275–278.
3. Smith BL, et al. (1999) Molecular mechanistic origin of the toughness of natural adhesives, fibres and composites. *Nature* 399(6738):761–763.
4. Srinivasarao M (1999) Nano-optics in the biological world: Beetles, butterflies, birds, and moths. *Chem Rev* 99(7):1935–1962.
5. Vukusic P, Sambles JR (2003) Photonic structures in biology. *Nature* 424(6950): 852–855.
6. Kinoshita S, Yoshioka S, Miyazaki J (2008) Physics of structural colors. *Rep Prog Phys* 71(7):076401.
7. Kinoshita S, Yoshioka S, Kawagoe K (2002) Mechanisms of structural colour in the Morpho butterfly: Cooperation of regularity and irregularity in an iridescent scale. *Proc Biol Sci* 269(1499):1417–1421.
8. Luke SM, Hallam BT, Vukusic P (2010) Structural optimization for broadband scattering in several ultra-thin white beetle scales. *Appl Opt* 49(22):4246–4254.
9. Stavenga DG, Leertouwer HL, Marshall NJ, Osorio D (2011) Dramatic colour changes in a bird of paradise caused by uniquely structured breast feather barbules. *Proc R Soc B Biol Sci* 278(1715):2098–2104.
10. Shawkey MD, Hill GE (2006) Significance of a basal melanin layer to production of non-iridescent structural plumage color: Evidence from an amelanotic Steller's jay (Cyanocitta stelleri). *J Exp Biol* 209(Pt 7):1245–1250.
11. Pfaff G, Reynders P (1999) Angle-dependent optical effects deriving from submicron structures of films and pigments. *Chem Rev* 99(7):1963–1982.
12. Klupp Taylor RN, et al. (2011) Painting by numbers: Nanoparticle-based colorants in the post-empirical age. *Adv Mater* 23(22–23):2554–2570.
13. Galisteo-López JF, et al. (2011) Self-assembled photonic structures. *Adv Mater* 23(1): 30–69.
14. Vogel N, Weiss CK, Landfester K (2012) From soft to hard: The generation of functional and complex colloidal monolayers for nanolithography. *Soft Matter* 8(15): 4044–4061.
15. von Freymann G, Kitaev V, Lotsch BV, Ozin GA (2013) Bottom-up assembly of photonic crystals. *Chem Soc Rev* 42(7):2528–2554.
16. Velev OD, Lenhoff AM, Kaler EW (2000) A class of microstructured particles through colloidal crystallization. *Science* 287(5461):2240–2243.
17. Yi GR, et al. (2002) Monodisperse micrometer-scale spherical assemblies of polymer particles. *Adv Mater* 14(16):1137–1140.
18. Brugarolas T, Tu F, Lee D (2013) Directed assembly of particles using microfluidic droplets and bubbles. *Soft Matter* 9(38):9046–9058.
19. Zhao Y, Shang L, Cheng Y, Gu Z (2014) Spherical colloidal photonic crystals. *Acc Chem Res* 47(12):3632–3642.
20. Bausch AR, et al. (2003) Grain boundary scars and spherical crystallography. *Science* 299(5613):1716–1718.
21. Meng G, Paulose J, Nelson DR, Manoharan VN (2014) Elastic instability of a crystal growing on a curved surface. *Science* 343(6171):634–637.
22. de Nijs B, et al. (2015) Entropy-driven formation of large icosahedral colloidal clusters by spherical confinement. *Nat Mater* 14(1):56–60.
23. Kim SH, Lee SY, Yi GR, Pine DJ, Yang SM (2006) Microwave-assisted self-organization of colloidal particles in confining aqueous droplets. *J Am Chem Soc* 128(33): 10897–10904.
24. Kim SH, Jeon SJ, Yang SM (2008) Optofluidic encapsulation of crystalline colloidal arrays into spherical membrane. *J Am Chem Soc* 130(18):6040–6046.
25. Yu Z, Wang CF, Ling L, Chen L, Chen S (2012) Triphase microfluidic-directed self-assembly: Anisotropic colloidal photonic crystal supraparticles and multicolor patterns made easy. *Angew Chem Int Ed Engl* 51(10):2375–2378.
26. Kim S-H, Park J-G, Choi TM, Manoharan VN, Weitz DA (2014) Osmotic-pressure-controlled concentration of colloidal particles in thin-shelled capsules. *Nat Commun* 5:3068.
27. Xie Z, et al. (2014) An optical nose chip based on mesoporous colloidal photonic crystal beads. *Adv Mater* 26(15):2413–2418.
28. Kim J, et al. (2011) Real-time optofluidic synthesis of magnetochromatic microspheres for reversible structural color patterning. *Small* 7(9):1163–1168.
29. Zhao X, et al. (2006) Colloidal crystal beads as supports for biomolecular screening. *Angew Chem Int Ed Engl* 45(41):6835–6838.
30. Liu W, et al. (2014) Photonic crystal encoded microcarriers for biomaterial evaluation. *Small* 10(1):88–93.
31. Utada AS, et al. (2007) Dripping, jetting, drops, and wetting: The magic of microfluidics. *MRS Bull* 32(09):702–708.
32. Anna SL, Bontoux N, Stone HA (2003) Formation of dispersions using "flow focusing" in microchannels. *Appl Phys Lett* 82(3):364–366.
33. Phillips KR, et al. (2014) Tunable anisotropy in inverse opals and emerging optical properties. *Chem Mater* 26(4):1622–1628.
34. Aguirre CI, Reguera E, Stein A (2010) Colloidal photonic crystal pigments with low angle dependence. *ACS Appl Mater Interfaces* 2(11):3257–3262.
35. Pursiainen OL, et al. (2007) Nanoparticle-tuned structural color from polymer opals. *Opt Express* 15(15):9553–9561.
36. Eustis S, el-Sayed MA (2006) Why gold nanoparticles are more precious than pretty gold: Noble metal surface plasmon resonance and its enhancement of the radiative and nonradiative properties of nanocrystals of different shapes. *Chem Soc Rev* 35(3): 209–217.
37. Koay N, et al. (2014) Hierarchical structural control of visual properties in self-assembled photonic-plasmonic pigments. *Opt Express* 22(23):27750–27768.
38. Rastogi V, et al. (2008) Synthesis of light-diffracting assemblies from microspheres and nanoparticles in droplets on a superhydrophobic surface. *Adv Mater* 20(22): 4263–4268.
39. Palmer C (2005) *Diffraction Grating Handbook* (Newport Corporation, Rochester, NY).
40. Vogel N, Goerres S, Weiss CK, Landfester K (2011) A convenient method to produce close-packed and non-close-packed monolayers using direct assembly of colloids at the air-water interface. *Macromol Chem Phys* 212(212):1719–1734.
41. Vogel N, de Viguerie L, Jonas U, Weiss C, Landfester K (2011) Wafer-scale fabrication of ordered binary colloidal monolayers with adjustable stoichiometries. *Adv Funct Mater* 21(16):3064–3073.
42. Fernández-López C, et al. (2009) Highly controlled silica coating of PEG-capped metal nanoparticles and preparation of SERS-encoded particles. *Langmuir* 25(24): 13894–13899.
43. Kubo S, et al. (2007) Tunability of the refractive index of gold nanoparticle dispersions. *Nano Lett* 7(11):3418–3423.